Physica Scripta

INCLUSIVE PUBLISHING TRUSTED SCIENCE
PURPOSE-LED PUBLISHING™

PAPER • **OPEN ACCESS**

Pairing correlation effects on Gamow–Teller strengths and β-decay properties of ^{74}Kr

To cite this article: Sadiye Meral Cakmak 2026 *Phys. Scr.* **101** 245303

View the article online for updates and enhancements.

You may also like

- Invariant shock-wave solutions in an equatorial shallow-water model
Ranis Ibragimov and Kennedy Byrd
- An accurate variational basis set for confined hydrogen atom
Deepak Singh and Rabeet Singh
- Geometry-controlled spin-wave spectra and mode filtering in helicoidal permalloy nanowires
Piero Terruzzi, Eduardo Saavedra, David Laroze et al.

This content was downloaded from IP address 193.140.141.192 on 22/06/2026 at 22:07

Physica Scripta

Check for updates

OPEN ACCESS

RECEIVED
12 March 2026

REVISED
21 May 2026

ACCEPTED FOR PUBLICATION
5 June 2026

PUBLISHED
16 June 2026

Original content from this work may be used under the terms of the Creative Commons Attribution 4.0 licence.

Any further distribution of this work must maintain attribution to the author(s) and the title of the work, journal citation and DOI.

PAPER

Pairing correlation effects on Gamow–Teller strengths and β-decay properties of ^{74}Kr

Sadiye Meral Cakmak*

Program of Medical Imaging Techniques, Osmangazi University, Eskisehir, Türkiye
* Author to whom any correspondence should be addressed.

E-mail: scakmak@ogu.edu.tr

Keywords: Gamow–Teller strengths, β-decay, pairing correlations, half-lives, QRPA

Abstract

This study investigates how neutron and proton pairing correlations influence the Gamow–Teller (GT) strength distributions and β-decay properties of ^{74}Kr for both spherical and deformed nuclear configurations. Unlike previous quasiparticle random phase approximation (QRPA) studies of ^{74}Kr that mainly emphasized deformation effects, the present work systematically investigates how different experimentally constrained pairing-gap prescriptions affect GT strength distributions and weak-decay observables within a unified spherical and deformed QRPA framework. Instead of treating pairing gaps as adjustable parameters, we employ three prescriptions constrained by experimental data (mass-dependent gaps, AME2020 odd–even staggering, and separation-energy–based gaps) to evaluate the sensitivity of GT and β-decay observables to realistic pairing inputs. Pairing correlations modify quasiparticle energies and configuration mixing within the QRPA framework, leading to changes in centroid energies, fragmentation patterns, and transition strengths. The analysis is performed within the QRPA formalism. Spherical calculations are carried out using the schematic model (SM-sph) and the Pyatov method. Deformed-basis calculations are performed for both oblate and prolate configurations using the SM and, for reference, within the single-quasiparticle approximation , in order to evaluate the influence of different neutron (Δ_n) and proton (Δ_p) pairing gaps. The results show that pairing correlations significantly modify the GT strength distributions, producing model-dependent shifts in peak positions and strength values. Furthermore, β-decay observables such as log(ft) values and half-lives in the deformed configurations exhibit a strong sensitivity to the pairing input. These findings highlight the importance of incorporating realistic pairing effects in nuclear models to achieve reliable predictions of weak-interaction processes and to improve the understanding of nuclear structure in both spherical and deformed systems. The calculated results reproduce the available experimental GT data without introducing an additional phenomenological quenching factor for the axial-vector coupling constant. However, this result should be regarded as model dependent and specific to the present QRPA framework and the considered observables of ^{74}Kr.

1. Introduction

Gamow–Teller (GT) transitions are fundamental to the study of nuclear structure and weak interaction phenomena. They are particularly relevant in processes including β-decay, electron capture (EC), and interactions between neutrinos and nuclei, where spin–isospin operators play a mediating role. These transitions serve as a probe for both single-particle and collective nuclear dynamics. However, experimental GT strength distributions frequently deviate from predictions based on the independent particle model, mainly due to complex nuclear correlations. Among these, pairing correlations have a particularly strong influence [1, 2].

© 2026 The Author(s). Published by IOP Publishing Ltd

Pairing correlations, originating from the attractive interaction between nucleons occupying time-reversed states, are a central feature of the nuclear many-body problem. They are especially significant in open-shell nuclei, where nucleons form Cooper-like pairs that can substantially modify GT strength distributions [3, 4]. The presence of pairing can lead to a reduction (quenching) of the total GT strength [5], a shift in the centroid of the distribution, and a fragmentation of the strength over several transitions. Paar *et al* [6] investigated GT strength fragmentation within the quasiparticle random phase approximation (QRPA) framework, while Caurier *et al* [7] demonstrated the importance of configuration mixing using large-scale shell-model calculations. Such effects are particularly important in astrophysical environments, including core-collapse supernovae and neutron star crusts. Schatz *et al* [8] discussed the role of weak interactions in rp-process nucleosynthesis under extreme astrophysical conditions. Marketin *et al* [9] performed large-scale calculations of β-decay rates relevant to r-process nuclei, while Mustonen and Engel [10] investigated global β-decay properties within the QRPA framework.

The present study focuses on how pairing interactions shape GT strength distributions, with particular attention to their quenching, centroid shifts, and fragmentation patterns. For the case of ^{74}Kr, pairing correlations are a key factor affecting both the total GT strength and its distribution over final states. These correlations redistribute GT strength, spreading it across multiple transitions, which lowers the strength available for any single β-decay branch, effectively increasing the half-life [11, 12]. Moreover, the interplay between pairing and shell effects causes shifts in the centroid of the GT distribution [4, 6]. Theoretical investigations, including large-scale shell-model calculations and QRPA approaches, have shown that incorporating pairing correlations is crucial for reproducing the observed β-decay properties of ^{74}Kr. Otsuka *et al* [13] emphasized the importance of spin–isospin interactions in exotic nuclei, while Bender *et al* [14] reviewed self-consistent mean-field approaches for nuclear structure studies. In addition, Niu *et al* [15] investigated β-decay half-lives within a QRPA-based framework.

In microscopic descriptions of β-transition strengths, spherical single-particle bases are commonly used within the quasiparticle random phase approximation (QRPA) framework for nuclei close to spherical symmetry. In the present work, the schematic model (SM) and the Pyatov method (PM) are treated as two realizations of the same QRPA formalism. For permanently deformed nuclei, quasiparticle states are generated from an axially deformed mean-field potential, leading to additional configuration mixing and GT fragmentation. In recent decades, numerous microscopic approaches have been proposed to represent β-strength distributions using both spherical and deformed bases, together with pairing and residual spin–isospin interactions. Early studies using the QRPA [16] combined with the Nilsson model [17] laid the foundation for deformation effects. Subsequent frameworks have incorporated Woods–Saxon single-particle potentials [18], separable interactions in Hartree–Fock [19, 20], energy-density functionals [21], and self-consistent models for neutron-rich nuclei [22]. Shell-model studies [7, 23] have further confirmed the decisive role of deformation in shaping GT distributions. Frisk *et al* [19] investigated GT β^+ decay in deformed nuclei near the proton drip line, while Hamamoto and Zhang [20] examined the shape dependence of GT decay in proton-rich nuclei. Sarriguren *et al* [24] studied shape isomerism and β-decay in ^{74}Kr, and later extended these investigations to odd-A and even–even krypton isotopes [25].

For ^{74}Kr, experimental measurements of GT strength distributions at CERN/ ISOLDE have provided strong evidence for ground-state shape mixing [26, 27]. Both theoretical and experimental investigations have revealed that this nucleus exhibits pronounced shape coexistence and mixing. Petrovici *et al* [28] investigated microscopic aspects of shape coexistence in krypton isotopes, while earlier studies by the same group analyzed shape transitions in nuclei from krypton to molybdenum [29]. Experimental evidence for a highly deformed oblate state in ^{74}Kr was reported by Chandler *et al* [30]. In addition, Petrovici *et al* [31] reviewed shape coexistence phenomena in medium-mass nuclei. The measured electric monopole (E_0) transitions are also consistent with theoretical predictions. Petrovici *et al* [28, 29, 31] discussed shape coexistence and mixing effects in krypton nuclei, while Bender and Heenen [32] investigated configuration mixing within the Skyrme energy-density-functional framework.

Systematic studies of log(ft) values in β-decay have contributed significantly to the understanding of weak-interaction properties. Gleit *et al* [33] provided early compilations of β-decay transition probabilities, while Raman and Gove [34] discussed spin and parity assignments based on log(ft) values. Singh *et al* [35] later reviewed experimental log(ft) systematics in detail. More recent work, such as the self-consistent study of GT β-decay in ^{74}Kr by Petrovici *et al* [36] and investigations of krypton isotopes within the Hartree–Fock + Bardeen–Cooper–Schrieffer (HF+BCS) pairing framework by Sarriguren and collaborators [24, 25], have further advanced this field. However, a systematic comparison of experimentally constrained pairing-gap prescriptions within both spherical and deformed QRPA realizations for ^{74}Kr remains limited. In addition, Nabi and collaborators have investigated how pairing correlations influence the half-lives associated with β-decay in fp-shell nuclei [37]. Building on these advances, the present work examines the influence of pairing effects on GT strength distributions and on the β-decay

behavior of ^{74}Kr, with an emphasis on shape coexistence and mixing phenomena. The theoretical framework involves PM [38] and a SM, enabling the comparison of deformed and spherical configurations. The computed half-lives and log(ft) values are contrasted with experimental measurements to assess how well the theoretical models perform. Previous QRPA studies of ^{74}Kr mainly focused on deformation effects. In contrast, the present work systematically investigates how different experimentally constrained pairing-gap prescriptions influence GT strength distributions and weak-decay observables within a unified spherical and deformed QRPA framework. In particular, three different pairing prescriptions, namely the mass-dependent formula, AME2020 odd–even mass differences, and separation-energy-based expressions, are consistently tested for spherical, prolate, and oblate configurations. This enables a direct analysis of the interplay between nuclear deformation and pairing correlations in shaping GT fragmentation patterns, centroid energies, log(ft) values, and total ($\beta^+ + \mathrm{EC}$) half-lives.

The remainder of this paper is organized as follows. Section 2 presents the theoretical formalism employed in the calculations. Section 3 discusses the calculated GT strength distributions and the corresponding β-decay properties. Finally, the main results and conclusions of the present study are summarized in section 4.

2. Theoretical formalism

In this part, the core formalism of the SM and the PM, as applied within the QRPA framework in this study, is outlined. The models describe nucleons moving in a mean field and include pairing correlations, spin–isospin couplings, and charge–exchange components.

To avoid ambiguity in terminology, all calculations in this work are performed within the QRPA formalism. The SM and the PM represent two realizations of this framework, with the latter including an additional symmetry-restoring term h_0.

The labels 'spherical' and 'deformed' refer solely to the choice of the underlying (quasi)particle basis generated from a spherical or axially deformed mean field. Accordingly, SM-sph and PM-sph denote calculations performed in a spherical basis, whereas SM-def and single–quasiparticle approximation (SQP-def) correspond to calculations carried out in a deformed basis. In addition, we employ the SQP, obtained by retaining only H_{SQP}, which already includes pairing correlations at the BCS level, and by neglecting the residual particle–hole (ph) and particle–particle (pp) interactions beyond the mean field. SQP results in a deformed basis are labeled SQP-def. This unified treatment enables a systematic investigation of pairing effects on GT strength distributions, β-decay characteristics, and related observables.

In the SM, the Hamiltonian is expressed in the quasiparticle representation as

$$H_{\mathrm{SM}} = H_{\mathrm{SQP}} + h_{\mathrm{ph}} + h_{\mathrm{pp}}, \tag{1}$$

where H_{SQP} denotes the Hamiltonian for a single quasiparticle

$$H_{\mathrm{SQP}} = \sum_{s,\tau,\rho} E_s(\tau)\, \alpha^{\dagger}_{s\rho}\alpha_{s\rho} \qquad \tau = n,p \tag{2}$$

Here, $E_s(\tau)$ is the single-quasiparticle energy, and $\alpha^{\dagger}_{s\rho}$, $\alpha_{s\rho}$ are creation and annihilation operators.

In equation (6), s denotes the single–quasiparticle level index and $\rho = \pm\frac{1}{2}$ corresponds to the projection of the nucleon spin on the symmetry axis, which gives rise to Kramers' degeneracy in axially symmetric systems. The quasiparticle energies $E_s(\tau)$ for neutrons ($\tau = n$) and protons ($\tau = p$) follow from the BCS solution,

$$E_s(\tau) = \sqrt{(\epsilon_s(\tau) - \lambda_\tau)^2 + \Delta_\tau^2}, \tag{3}$$

where $\epsilon_s(\tau)$ is the single–particle energy obtained from the Woods–Saxon potential, λ_τ is the corresponding Fermi level, and Δ_τ represents the neutron or proton pairing gap. The GT effective interaction terms, corresponding to the ph and pp channels, are defined by

$$\begin{aligned} h^{\mathrm{GT}}_{\mathrm{ph}} &= 2\chi^{\mathrm{GT}}_{\mathrm{ph}}\Sigma_\mu \beta^+_\mu \beta^-_\mu, \\ h^{\mathrm{GT}}_{\mathrm{pp}} &= -2\kappa^{\mathrm{GT}}_{\mathrm{pp}}\Sigma_\mu P^+_\mu P^-_\mu, \qquad \mu = 0, \pm 1; \end{aligned} \tag{4}$$

with

$$\beta^+_\mu = \sum_{n,p,\rho,\rho'} \langle n\rho|\sigma_\mu + (-1)^\mu \sigma_{-\mu}|p\rho'\rangle \alpha^{\dagger}_{\mathrm{np}}\alpha_{p\rho'}, \beta^-_\mu = \left(\beta^+_\mu\right)^{\dagger},$$

$$P_{\mu}^{+}=\sum_{n,p,\rho,\rho^{'}}\langle n\rho|\sigma_{\mu}+(-1)^{\mu}\sigma_{-\mu}|p\rho^{'}\rangle\alpha_{\mathrm{np}}^{\dagger}\alpha_{p\rho^{'}}^{\dagger},P_{\mu}^{-}=\left(P_{\mu}^{+}\right)^{\dagger}. \tag{5}$$

Here, κ_{pp} represents the pp interaction strength in the spin–isospin channel, whereas χ_{ph} corresponds to the ph interaction strength responsible for the repulsive GT force that governs the position of the GT resonance. $\alpha_{\mathrm{np}}^{\dagger}$ denotes a shorthand notation for neutron–proton two–quasiparticle creation operators, which are later expressed explicitly in terms of the $D_{\mathrm{np}}^{\dagger}$ operators within the QRPA phonon construction.

In this context, σ_{μ} represents the spherical components of the Pauli matrices. When transformed into the quasiparticle representation, the operators $\beta_{\mu}^{\pm}$ and $P_{\mu}^{\pm}$ can be expressed through quasiparticle scattering operators (D_{np}) and neutron–proton pair creation/annihilation operators ($C_{\mathrm{np}}^{\dagger}$, C_{np}). Under the quasiboson approximation, these operators satisfy bosonic commutation relations, allowing the effective GT interactions to be separated into *CC*, *DD*, and *CD* contributions [39].

In equation (11), V_c, V_{ls}, and V_1 correspond, respectively, to the central, spin–orbit, and isovector components of the mean field. These terms break the commutation of the GT operator with the underlying single–particle Hamiltonian. Within the PM, the additional correction term h_0 is introduced to restore the broken commutation symmetry between the GT operator and the mean-field Hamiltonian.

$$\left[H_{\mathrm{SQP}}-\left(V_c+V_{ls}+V_1\right),G_{1\mu}^{\rho}\right]=0. \tag{6}$$

Accordingly, the explicit form of h_0 is constructed as

$$h_0=\sum_{\rho=\pm}\frac{1}{2\gamma_{\rho}}\sum_{\mu=0,\pm1}\left[H_{\mathrm{SQP}}-V_c-V_{ls}-V_1,G_{1\mu}^{\rho}\right]^{\dagger}\left[H_{\mathrm{SQP}}-V_c-V_{ls}-V_1,G_{1\mu}^{\rho}\right], \tag{7}$$

where γ_{ρ} is determined from the corresponding commutation relations [40, 41]:

$$\gamma_{\rho}=\frac{\rho}{2}\langle0|\left[\left[H_{\mathrm{sqp}}-\left(V_c+V_{ls}+V_1\right),G_{1\mu}^{\rho}\right],G_{1\mu}^{\rho}\right]|0\rangle. \tag{8}$$

The inclusion of h_0 guarantees that the GT operator remains a conserved generator of spin–isospin symmetry in the intrinsic nuclear frame, compensating for the symmetry breaking originating from V_c, V_{ls}, and V_1 components of the mean field.

This expression follows the standard Pyatov prescription and is equivalent to the double-commutator form used in earlier works, differing only in notation. The GT transition operator is given by:

$$G_{1\mu}^{\pm}=\frac{1}{2}\sum_{k=1}^{A}\left[\sigma_{1\mu}(k)\,t^{+}(k)+\rho\,(-1)^{\mu}\,\sigma_{1,-\mu}(k)\,t^{-}(k)\right],\qquad(\rho=\pm1), \tag{9}$$

where $\sigma_{1\mu}(k)=2s_{1\mu}(k)$ are the spherical components of the Pauli spin operators, and $t^{\pm}(k)=t_x(k)\pm it_y(k)$ denote the isospin raising and lowering operators, respectively.

Here, the combination $\sigma_{1\mu}(k)+(-1)^{\mu}\sigma_{1-\mu}(k)$ is written in a spherical-tensor form to ensure the correct hermiticity and transformation properties of the spin operator in the spherical basis (with $\sigma_{1\mu}=2s_{1\mu}$).

The complete Hamiltonian within the PM framework can be written as

$$H_{\mathrm{PM}}=H_{SQP}+h_0+h_{\mathrm{ph}}+h_{\mathrm{pp}}. \tag{10}$$

Subsequently, the GT transition strengths are evaluated using

$$B_{\mathrm{GT}}^{(\pm)}(\omega_i)=\sum_{\mu}\left|\langle1_{i,\mu}^{+}|G_{1\mu}^{\pm}|0^{+}\rangle\right|^{2}, \tag{11}$$

where ω_i is the excitation energy in the daughter nucleus.

In both SM and PM approaches, the $|1_i^{+}\rangle$ excited states are constructed as QRPA phonons built upon the BCS ground state,

$$|1_i^{+}\rangle=Q_{1_i^{+}}^{\dagger}|0^{+}\rangle, \tag{12}$$

where the phonon operator takes the form

$$Q^{\dagger}_{1^{+}_{i}} = \sum_{n,p} \left[X^{(i)}_{\mathrm{np}} D^{\dagger}_{\mathrm{np}} - Y^{(i)}_{\mathrm{np}} D_{\mathrm{np}} \right]. \tag{13}$$

Here, $D^{\dagger}_{\mathrm{np}}$ creates neutron–proton quasiparticle excitations, and the amplitudes $X^{(i)}_{\mathrm{np}}$ and $Y^{(i)}_{\mathrm{np}}$ are obtained by solving the QRPA dispersion relation. The only difference between SM and PM lies in the inclusion of the symmetry–restoring term h_0 in the PM basis, which modifies the quasiparticle interaction matrix elements. The summed strengths are

$$B(\mathrm{GT})_{\pm} = \sum_{i} B^{(\pm)}_{\mathrm{GT}}(\omega_i), \tag{14}$$

which must satisfy the Ikeda sum rule [42]:

$$B(\mathrm{GT})_{-} - B(\mathrm{GT})_{+} \approx 3(N-Z). \tag{15}$$

Although the Ikeda sum rule is exactly satisfied within QRPA when the full two–quasiparticle configuration space is included, a slight deviation may appear in practical calculations. This discrepancy arises from the finite configuration space employed in the present work, together with the truncation of weakly–occupied orbitals near the particle continuum. Such truncations reduce the summed $B(\mathrm{GT})$ values, leading to a small departure from the exact $3(N-Z)$ limit. The primary difference between the PM and SM lies in the inclusion of h_0 in the PM, which restores broken symmetries, whereas the SM omits this term [39, 43–46].

Pairing gaps are a key input in QRPA calculations. In this work, three prescriptions are tested:

1. A mass-dependent constant gap, $\Delta_p = \Delta_n = 12/\sqrt{A}$ MeV, with results labeled $\mathrm{PM}-\mathrm{sph}^{1}$, $\mathrm{SM}-\mathrm{sph}^{1}$, and $\mathrm{SM}-\mathrm{def}^{1}$.

2. Pairing gaps were determined using a symmetric five-point relation applied to odd–even mass differences, with experimental binding energies taken from the AME2020 evaluation [47]. The resulting values are labeled as $\mathrm{PM}-\mathrm{sph}^{2}$, $\mathrm{SM}-\mathrm{sph}^{2}$, and $\mathrm{SM}-\mathrm{def}^{2}$. This second expression involves five distinct binding energy (BE) values and can be written as:

$$\begin{aligned}\Delta_n &= \frac{1}{8}\left[\mathrm{BE}(N-2,Z) - 4\mathrm{BE}(N-1,Z) + 6\mathrm{BE}(N,Z) - 4\mathrm{BE}(N+1,Z) + \mathrm{BE}(N+2,Z)\right]\\ \Delta_p &= \frac{1}{8}\left[\mathrm{BE}(N,Z-2) - 4\mathrm{BE}(N,Z-1) + 6\mathrm{BE}(N,Z) - 4\mathrm{BE}(N,Z+1) + \mathrm{BE}(N,Z+2)\right]\end{aligned} \tag{16}$$

3. Gaps determined from three-term expressions involving proton and neutron separation energies [48], with results labeled $\mathrm{PM}-\mathrm{sph}^{3}$, $\mathrm{SM}-\mathrm{sph}^{3}$, $\mathrm{SM}-\mathrm{def}^{3}$. Here, the expression is derived based on proton and neutron separation energies, formulated as:

$$\Delta_{\mathrm{n}} = \frac{(-1)^{A-Z+1}}{4}\left[S_{\mathrm{n}}(Z,A+1) - 2S_{\mathrm{n}}(Z,A) + S_{\mathrm{n}}(Z,A-1)\right], \tag{17}$$

$$\Delta_{\mathrm{p}} = \frac{(-1)^{Z+1}}{4}\left[S_{\mathrm{p}}(Z+1,A+1) - 2S_{\mathrm{p}}(Z,A) + S_{\mathrm{p}}(Z-1,A-1)\right]. \tag{18}$$

This multi-prescription approach allows one to assess how the calculated GT strength distributions, half-life values, and $\log(ft)$ results respond to variations in the pairing input. The three prescriptions are introduced to distinguish (i) a widely used global empirical estimate based on a mass-dependent gap, (ii) pairing gaps directly constrained by experimental odd–even mass staggering using AME2020 binding energies, and (iii) a complementary estimate derived from local separation-energy systematics. In this sense, the pairing interaction is not treated as a free tuning parameter; rather, the aim is to quantify how different experimentally grounded pairing inputs propagate into the SM and PM predictions of GT strength distributions and β-decay observables. For ^{74}Kr, the three prescriptions yield pairing gaps within a relatively narrow interval ($\Delta \approx 1.4$–1.7 MeV); nevertheless, they correspond to distinct experimental constraints and lead to non-negligible changes in peak positions, centroid energies, fragmentation patterns, and half-life values, as discussed in section 3.

Table 1. The neutron (Δ_n) and proton (Δ_p) pairing gaps (MeV) are given in the second and third columns, respectively. The fourth column lists the total GT$^+$ strength in units of $[g_A^2/4\pi]$, the fifth column shows the centroid energies $\overline{E}^+$ (MeV), and the last column presents the energy-weighted summed strength in units of [MeV $g_A^2/4\pi$], evaluated up to a cutoff energy of $E_{\rm cut} = 30$ MeV. The deformed-basis results (SM-def) are shown separately for the $K = 0$ and $K = 1$ (values in parentheses) components, where '(p)' and '(o)' denote the prolate and oblate configurations, respectively.

Models	Δ_n	Δ_p	$\sum B^+_{\rm GT}$	$\overline{E}^+$	$\sum {\rm EB}^+_{\rm GT}$
SM-def^3 (p)	1.739	1.675	2.560(5.74)	7.34(6.68)	19.25(17.21)
SM-def^2 (p)	1.681	1.581	2.564(5.86)	7.17(6.33)	17.99(16.26)
SM-def^1 (p)	1.395	1.395	2.31(5.43)	6.48(5.66)	16.81(14.29)
SM-def^3 (o)	1.739	1.675	2.13(4.48)	7.61(7.81)	33.72(30.33)
SM-def^2 (o)	1.681	1.581	2.03(4.38)	7.37(7.63)	34.17(29.33)
SM-def^1 (o)	1.395	1.395	1.96(3.13)	6.49(7.20)	28.91(33.07)
SM-sph^3	1.739	1.675	4.59	6.65	40.63
SM-sph^2	1.681	1.581	4.42	6.47	40.49
SM-sph^1	1.395	1.395	3.88	6.14	42.33
PM-sph^3	1.739	1.675	0.51	6.91	28.07
PM-sph^2	1.681	1.581	0.53	7.20	27.11
PM-sph^1	1.395	1.395	0.48	8.02	30.69

Note: Superscripts ^{1}, ^{2}, and ^{3} indicate pairing gaps obtained from (1) the constant mass-dependent formula $\Delta_p = \Delta_n = 12/\sqrt{A}$, (2) experimental binding-energy differences, and (3) three-point separation-energy expressions, respectively.

3. GT strength distributions

The influence of different neutron and proton pairing gaps on the GT (β-decay) properties of ^{74}Kr has been investigated for both spherical and deformed configurations. All calculations in this work are performed within the same QRPA formalism, using different realizations of the schematic interaction. For spherical configurations, calculations are carried out within the SM-sph and the PM-sph, while the deformed configuration is treated within the same schematic QRPA framework adopted throughout this work, using a deformed SM (SM-def) and single-quasiparticle (SQP-def).

For the deformed configuration (SM-def and SQP-def), the single–particle levels are generated from a deformed Woods–Saxon potential. Residual spin–isospin interactions are included in both the ph and pp channels, with interaction strengths $\chi_{\rm ph}$ and $\kappa_{\rm pp}$ fixed to their standard mass–dependent values, $\chi_{\rm ph} = 5.2A^{-0.7}$ and $\kappa_{\rm pp} = 0.58A^{-0.7}$ [49]. It is worth emphasizing that GT strength distributions are affected by both isovector pairing correlations (nn and pp), which are incorporated through the neutron and proton pairing gaps Δ_n and Δ_p, and residual spin–isospin interactions in the ph and pp channels, governed by the interaction strengths $\chi_{\rm ph}$ and $\kappa_{\rm pp}$, respectively. In the present work, both $\chi_{\rm ph}$ and $\kappa_{\rm pp}$ are kept fixed at their standard mass–dependent values in order to isolate and quantify specifically the impact of experimentally constrained pairing–gap prescriptions on GT strength distributions and β-decay observables. A systematic investigation of the sensitivity of GT strengths and half-lives to variations of $\chi_{\rm ph}$ and $\kappa_{\rm pp}$ represents a separate and complementary problem and is therefore beyond the scope of the present study. Here, $\kappa_{\rm pp}$ effectively controls the strength of the *pn* pp (isoscalar) channel in the adopted separable interaction. A dedicated investigation of the sensitivity of GT observables to the residual interaction strengths $\chi_{\rm ph}$ and $\kappa_{\rm pp}$ has already been addressed in our previous QRPA study of ^{74}Kr [50]. In contrast, the primary objective of the present work is to isolate and quantify the influence of different experimentally constrained pairing-gap prescriptions on GT strength distributions and β-decay observables while keeping the residual interaction sector fixed. This separation allows the specific role of pairing correlations to be analyzed without introducing additional parameter-dependent effects associated with the ph and pp residual interactions.

The deformation parameters (ϵ_2, β_2) are taken from the mass-table analysis of Möller *et al* [51, 52]. For the prolate configuration, the deformation parameter $\beta_2 = +0.2544$ is adopted, while the oblate configuration is obtained by using the same magnitude with opposite sign, $\beta_2 = -0.2544$. The resulting Nilsson-like states are eigenstates of the angular momentum projection K on the symmetry axis. Accordingly, the GT strengths in the deformed basis are calculated separately for the $K = 0$ and $K = 1$ components, as reported in table 1. The enhanced fragmentation observed in the deformed results originates from the mixing of Nilsson orbitals and the presence of multiple K components.

To highlight the specific role of the pairing input, we present the results in a prescription-by-prescription manner. The mass-dependent gap provides a global baseline, whereas the AME2020 five-point OES gaps represent the most direct experimental constraint on pairing correlations in the ground

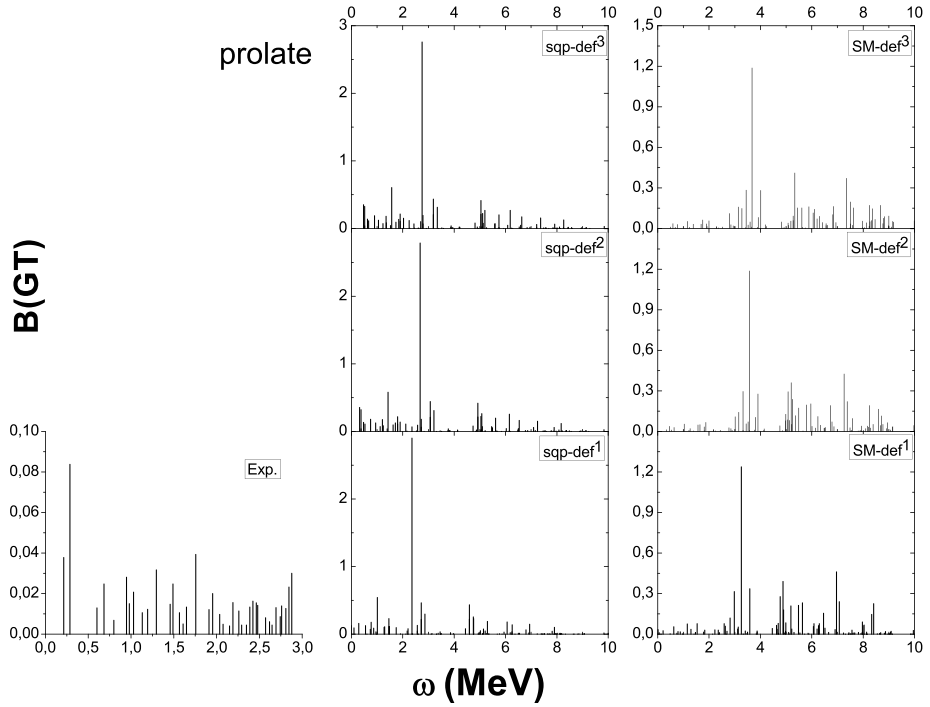


Figure 1. Gamow–Teller (GT) strength distributions $[g_A^2/4\pi]$ in the β^+ decay direction for **prolate-deformed** ^{74}Kr computed using three different neutron and proton pairing gaps within the SQP and SM frameworks. Larger pairing gaps shift the main GT peak to higher excitation energies and reduce the 1^+ strength. Experimental data from reference [27] are shown for comparison. This behavior indicates that stronger pairing correlations increase the fragmentation of the GT strength and reduce the collectivity of individual transitions.

state. The separation-energy-based gaps offer an alternative local indicator that is sensitive to the neighboring mass surface. Although the resulting gaps differ only moderately for ^{74}Kr, the GT response and β^+ observables show a measurable sensitivity to the underlying prescription, indicating that the choice of experimentally constrained pairing input is not a merely technical detail.

Comparisons among the three gap prescriptions show that the constant mass-dependent gap (superscript 1) yields the smallest values, while the separation-energy-based gaps (superscript 3) produce the largest ones (table 1). Here, superscripts ^{1}, ^{2}, and ^{3} denote pairing gaps derived from a constant mass-dependent formula, experimental binding-energy differences, and separation-energy expressions, respectively, corresponding to an increasing degree of microscopic input from nuclear masses.

From a microscopic point of view, the observed sensitivity of the GT strength distributions to the pairing gaps originates from the modification of the quasiparticle spectrum within the BCS framework. As shown in equation (7), increasing the neutron and proton pairing gaps (Δ_n, Δ_p) increases the quasiparticle energies near the Fermi surface, thereby shifting the dominant neutron–proton two–quasiparticle excitations to higher energies. Consequently, the centroid energies of the GT distributions are displaced toward higher excitation regions, particularly in the deformed configurations. At the same time, stronger pairing correlations enhance configuration mixing through the QRPA phonon amplitudes, redistributing the GT strength over a larger number of transitions instead of concentrating it in a few dominant peaks.

This mechanism naturally leads to increased fragmentation and to a reduction of the strongest individual GT transitions. In addition, the pairing-induced modification of the BCS occupation amplitudes (u, v) changes the underlying GT transition matrix elements, further affecting the balance between collectivity and fragmentation in both spherical and deformed bases.

Figure 1 displays the GT strength distributions obtained within the single-quasiparticle (SQP) and SM approaches for the **prolate-deformed** configuration of ^{74} Kr, together with the available experimental data [27]. In the SQP-def calculations, the main GT peak for SQP-def^1 appears at 2.357 MeV with a strength of 2.9013, while SQP-def^2 shifts this peak to 2.6742 MeV (strength 2.788) and SQP-def^3 to 2.7546 MeV (strength 2.7573). Within the SM-def framework, SM-def^1 predicts a dominant peak at 3.2511 MeV (1.2372), SM-def^2 at 3.5714 MeV (1.1881), and SM-def^3 at 3.6741 MeV (1.1874). In both approaches, increasing neutron and proton pairing gaps systematically shift the GT strength toward higher excitation energies. At the same time, the dominant 1^+ strength decreases because the

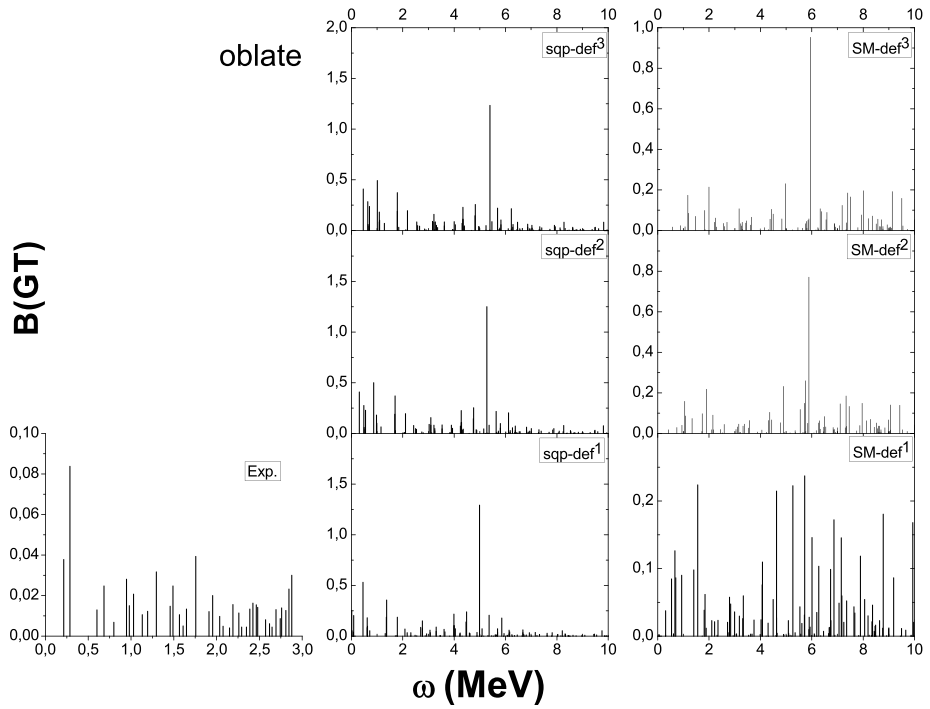


Figure 2. Gamow–Teller (GT) strength distributions $[g_A^2/4\pi]$ in the β^+ decay direction for **oblate-deformed** ^{74}Kr, computed using three different neutron and proton pairing gaps within the SQP and SM frameworks. As in the prolate case, increasing pairing gaps shift the dominant GT strength toward higher excitation energies and modify the 1^+ strength distribution. Experimental data from reference [27] are shown for comparison. The broader GT distribution in the oblate configuration suggests that deformation enhances the density of accessible quasiparticle configurations.

GT strength becomes redistributed over a larger number of neutron–proton two–quasiparticle configurations. This behavior reflects enhanced QRPA configuration mixing and increased quasiparticle energies near the Fermi surface.

Figure 2 shows the GT strength distributions obtained for the **oblate-deformed** configuration of ^{74}Kr within the SQP and SM approaches. In the SQP-def calculations, the dominant GT peak for SQP-def^1 appears at 4.9852 MeV with a strength of 1.2945. When the pairing gaps are increased according to the five-point odd–even mass differences (SQP-def^2), the main peak is shifted to 5.2768 MeV with a reduced strength of 1.2495, while the use of three-point SQP-def^3 further moves the peak to 5.3975 MeV and slightly decreases the strength to 1.2342. A similar systematic trend is observed within the SM-def framework. The main GT peak predicted by SM-def^1 is located at 5.7274 MeV with a strength of 0.2371, whereas SM-def^2 shifts this peak to 5.8912 MeV with an enhanced strength of 0.7704. For the largest pairing gaps (SM-def^3), the dominant peak is found at 5.9569 MeV with a strength of 0.9523. In both models, increasing neutron and proton pairing gaps lead to a gradual shift of the GT strength toward higher excitation energies. This behavior reflects the combined effect of stronger pairing correlations, which increase the quasiparticle energies, and the oblate deformation, which enhances the mixing of Nilsson orbitals and redistributes the GT strength over a broader energy range. The broader GT distribution observed in the oblate configuration indicates that deformation and pairing correlations act cooperatively to increase the density of accessible two–quasiparticle states. This contrast highlights the different sensitivity of the SQP and SM approaches to pairing correlations, with the SM framework exhibiting a more collective response in the oblate configuration.

Figure 3 compares **spherical** ^{74}Kr results from the PM and SM with experimental data [27]. In PM-sph, PM-sph^1 yields a main peak at 6.3744 MeV (0.2347), PM-sph^2 at 5.8312 MeV (0.2874), and PM-sph^3 at 5.6997 MeV (0.2931). In SM-sph, SM-sph^1 places the peak at 4.2009 MeV (1.2734), SM-sph^2 at 4.1400 MeV (1.2595), and SM-sph^3 at 4.0937 MeV (1.2033). For spherical shapes, peak energies generally shift lower with increasing gaps. Notably, in PM-sph the 1^+ GT strength increases with larger gaps, whereas in SM it decreases. This opposite trend reflects the different treatment of residual spin–isospin correlations and symmetry restoration in the PM and SM realizations. In the PM framework, the symmetry-restoring term modifies the balance between collectivity and fragmentation, allowing part of the GT strength to remain concentrated even for larger pairing gaps. Taken together, the results shown in figures 1–3 demonstrate that nuclear deformation plays a decisive role in shaping the GT strength

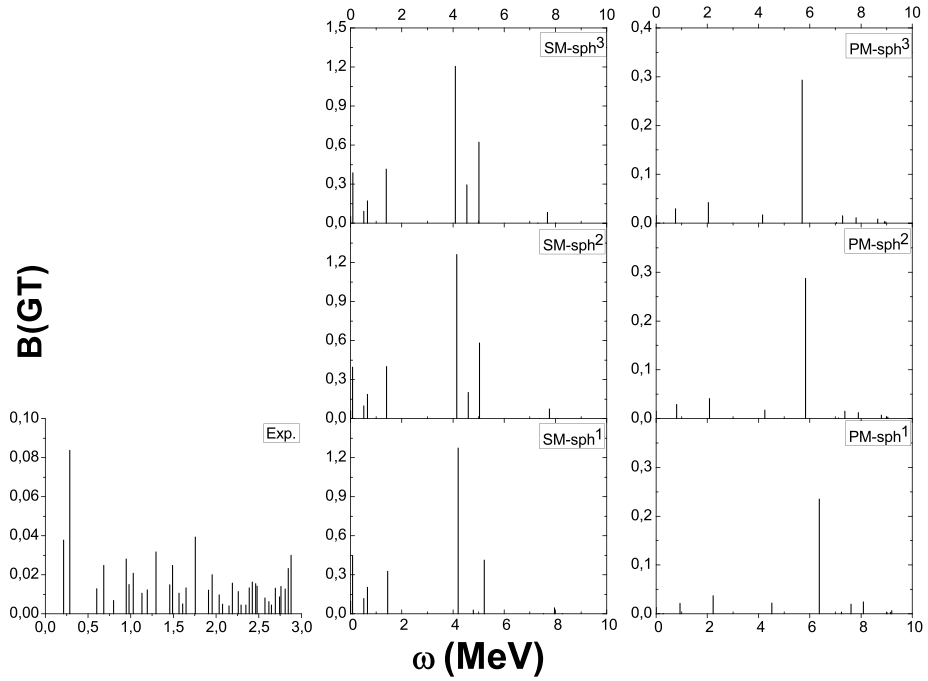


Figure 3. Calculated GT strength distributions $[g_A^2/4\pi]$ in the β^+ direction for **spherical** ^{74}Kr using three different pairing-gap prescriptions within the SM and PM frameworks. Increasing pairing gaps modify the centroid energies and fragmentation patterns of the GT strength distributions. Compared with the deformed calculations, the spherical results exhibit more concentrated GT strength distributions and weaker fragmentation effects. Experimental data from reference [27] are shown for comparison. The different trends observed between the PM and SM calculations reflect the sensitivity of GT collectivity to the treatment of symmetry restoration effects.

distributions of ^{74}Kr. Compared to the spherical calculations (figure 3), both prolate and oblate deformations (figures 1 and 2) lead to a pronounced fragmentation of the GT strength and shift the dominant transitions to higher excitation energies. Among the deformed configurations, the oblate shape exhibits a stronger redistribution of the GT strength over a broader energy range, reflecting enhanced mixing of Nilsson orbitals and increased collectivity, particularly within the SM-def framework.

In contrast, the spherical calculations display more concentrated GT strength distributions, with systematic but smaller energy shifts induced by pairing correlations. Overall, the deformed-basis calculations reproduce the experimental GT strength distributions more realistically in terms of energy placement, while the spherical PM approach yields a better description of the absolute GT strength. These findings highlight the interplay between nuclear shape and pairing correlations and underline the importance of deformation effects in describing GT transitions in shape-coexisting nuclei such as ^{74}Kr. A more detailed comparison with the available experimental GT strength distributions [27] indicates that the deformed-basis calculations provide an improved description of the excitation-energy region where the dominant GT strength is observed. In particular, the prolate and oblate SM-def results reproduce the experimental peak positions more accurately than the spherical SM and PM calculations. While the spherical PM approach yields GT strengths closer to the experimental magnitudes, it systematically places the dominant transitions at higher excitation energies. Overall, the present analysis suggests that nuclear deformation is essential for reproducing the experimental energy distribution of GT strength, whereas different model realizations exhibit complementary strengths in describing either the energy placement or the absolute GT strength. The deformed SM-def calculations reproduce the experimental GT peak positions within approximately 0.3–0.7 MeV, whereas the spherical PM calculations overestimate the excitation energies by nearly 2 MeV. This quantitative comparison confirms that nuclear deformation significantly improves the reproduction of the experimental GT energy distribution.

Table 1 summarizes the total GT$^+$ strength, centroid energies, and energy-weighted summed strengths for different neutron and proton pairing-gap prescriptions. For the deformed configurations, results are reported separately for the $K = 0$ and $K = 1$ components (the latter shown in parentheses), allowing one to disentangle the role of angular-momentum projection in shaping the GT strength distributions. In addition, the deformed-basis calculations are presented separately for the prolate (p) and oblate (o) shapes, revealing a clear shape dependence of the GT observables. For the prolate configuration within the SM-def framework, decreasing pairing gaps (Δ_n, Δ_p) lead to a systematic reduction of

Table 2. Calculated Ikeda sum-rule values for different pairing-gap prescriptions within the adopted QRPA frameworks. The exact Ikeda sum-rule limit for ^{74}Kr is $3(N-Z)=6$.

Model	$B(\mathrm{GT}^-)-B(\mathrm{GT}^+)$
SM-def^3 (p)	5.0707
SM-def^2 (p)	4.8712
SM-def^1 (p)	5.3395
SM-def^3 (o)	6.7421
SM-def^2 (o)	5.2033
SM-def^1 (o)	6.4550
SM-sph^3	5.6167
SM-sph^2	5.6059
SM-sph^1	5.6827
PM-sph^3	4.9771
PM-sph^2	5.4262
PM-sph^1	5.4878

Note: Superscripts ^{1}, ^{2}, and ^{3} denote pairing gaps obtained from (1) the constant mass-dependent formula, (2) experimental binding-energy differences, and (3) three-point separation-energy expressions, respectively.

both the centroid energies and the energy-weighted sums, indicating a concentration of GT strength at lower excitation energies. In contrast, the oblate configuration exhibits larger centroid energies and significantly enhanced energy-weighted sums, reflecting a stronger fragmentation of the GT strength and increased mixing of Nilsson orbitals. This enhancement is particularly pronounced for larger pairing gaps, where the oblate shape redistributes strength over a broader energy range. In the spherical limit, the SM-sph results show that decreasing pairing gaps reduce both the total GT strength and the centroid energies, while the PM-sph calculations display a different sensitivity, with centroids shifting to higher energies for smaller gaps. Overall, the comparison highlights that nuclear deformation—especially the oblate configuration—has a more pronounced impact on the GT centroids and energy-weighted sums than pairing correlations alone, underscoring the importance of shape effects in ^{74}Kr.

The calculated Ikeda sum-rule values obtained for the different pairing prescriptions are summarized in table 2. The results show that the adopted QRPA frameworks reproduce the Ikeda sum-rule limit, $3(N-Z)=6$, with moderate deviations depending on the pairing prescription and nuclear shape. The spherical SM and PM calculations remain relatively close to the exact limit, while somewhat larger variations are observed in the deformed SM results, particularly for the prolate and oblate configurations. These deviations can be attributed mainly to the finite two–quasiparticle model space and to the redistribution of GT strength within the adopted QRPA framework. Since the finite model space is expected to affect mainly the high-energy tail of the GT strength distribution, the low-energy region below the Q_{EC} window, which dominates the calculated $(\beta^+ + \mathrm{EC})$ decay observables, is comparatively less sensitive to this limitation.

The *ft* values corresponding to GT transitions are determined using

$$(ft)_{\beta^\mp} = \frac{D}{(g_A/g_V)^2\, 4\pi\, B_{\mathrm{GT}}\left(I_i \rightarrow I_f, \beta^\mp\right)}, \tag{19}$$

with $D = 6295$ s and $g_A/g_V = -1.254$ [53]. No phenomenological quenching factor is applied in the present calculations. In many shell-model and QRPA studies, effective reductions such as $g_{A,\mathrm{eff}} \approx (0.7\text{–}1.0)\, g_A$ are commonly introduced to reproduce experimental GT strengths and β-decay rates. Such quenching is generally associated with missing many-body correlations, truncated configuration spaces, meson-exchange currents, and configuration mixing beyond the adopted model space. In the present work, however, the calculated GT strength distributions, $\log(ft)$ values, and total $(\beta^+ + \mathrm{EC})$ half-lives already show satisfactory agreement with the available experimental data without introducing an additional reduction of g_A. Nevertheless, this behavior should be regarded as model dependent and nucleus dependent rather than as a universal conclusion. Fermi integrals are evaluated using the formulas in references [54, 55]. For proton-rich nuclei such as ^{74}Kr, both β^+ decay and EC are energetically allowed

and proceed through the same GT matrix elements. In the present work, the calculated half-lives correspond to the total weak-decay rate, obtained by summing the β^+ and EC contributions through the standard phase-space treatment. Accordingly, all $T_{1/2}$ values reported in table 4 refer to the combined (β^++ EC) half-life.

Branching ratios are obtained from

$$I = \frac{T_{1/2}}{t_{1/2}^{\mathrm{par}}} \times 100\,(\%)\,. \tag{20}$$

Within this context, $T_{1/2}$ refers to the overall half-life, whereas $t_{1/2}^{\mathrm{par}}$ specifies the partial value. The first nine columns of table 3 give log(ft) values and branching ratios for states below Q_{EC} obtained within the prolate-deformed SM framework, while the last three columns list the corresponding experimental data [48, 56]. In the SM-def[1] case, the use of equal neutron and proton pairing gaps leads to a stronger fragmentation of the GT strength below Q_{EC} compared to the other prescriptions. States with excitation energies $\omega < Q_{\mathrm{EC}}$ contribute to the total weak-decay rate through EC, whereas β^+ decay is energetically allowed only for states with $\omega < Q_{\beta^+} = Q_{\mathrm{EC}} - 2m_e c^2$.

Table 3 summarizes the GT transition energies, branching ratios, and log(ft) values for low-lying 1^+ states in the daughter nucleus ^{74}Br, obtained within the SM-def framework for the prolate-deformed configuration of ^{74}Kr. The results are presented separately for the $K = 0$ and $K = 1$ components, reflecting the axial symmetry of the deformed basis.

Overall, the calculated log(ft) values fall within the typical range for allowed GT transitions and show a reasonable agreement with the available experimental data. Transitions dominated by $K = 1$ components generally exhibit larger branching ratios, underlining the role of angular-momentum projection in shaping the decay pattern.

Among the three pairing prescriptions, the constant-gap case (SM-def[1]) produces a larger number of weak transitions with moderate log(ft) values, reflecting enhanced GT fragmentation below Q_{EC}. In contrast, pairing gaps derived from experimental binding energies (SM-def[2]) and separation energies (SM-def[3]) tend to concentrate the decay strength into fewer transitions, yielding log(ft) values closer to the experimental systematics. Most calculated log(ft) values differ from the experimental systematics by less than about 0.5–1.0 logarithmic units, which is acceptable for QRPA-based descriptions of GT transitions in deformed nuclei. The remaining discrepancies are likely associated with shape mixing effects and limitations of the truncated configuration space.

It should be noted that only the prolate configuration is considered in table 3, since the available experimental log(ft) values correspond to low-lying states that are commonly associated with the prolate minimum in ^{74}Kr.

Table 4 compares the calculated total (β^++ EC) half-lives of ^{74}Kr with the experimental value of 11.5 min [48, 57, 58], for both prolate and oblate deformed configurations. Overall, all three pairing-gap prescriptions yield half-lives in good agreement with experiment, confirming the reliability of the present QRPA-based description of weak decay in ^{74}Kr. For the prolate configuration, the half-life obtained with pairing gaps derived from experimental binding energies (SM-def[2], 11.54 min) provides the closest agreement with the experimental value, while the constant-gap case (SM-def[1]) slightly underestimates the half-life. A similar trend is observed for the oblate configuration, where SM-def[3] and SM-def[2] reproduce the experimental half-life within better than 5%, whereas SM-def[1] again yields shorter half-lives. In both shapes, the total half-life decreases systematically as the neutron and proton pairing gaps (Δ_n, Δ_p) are reduced, highlighting the sensitivity of the combined (β^++ EC) decay rate to pairing correlations. The close proximity of the prolate and oblate results further indicates that, although deformation strongly affects the GT strength distribution and fragmentation pattern, the integrated weak-decay half-life remains comparatively robust against shape changes in ^{74}Kr.

4. Summary and conclusions

In this work, the impact of neutron and proton pairing correlations on GT strength distributions and β^+-decay properties of ^{74}Kr has been systematically investigated for both spherical and deformed nuclear configurations. All calculations were performed within a unified QRPA framework, employing different realizations of the schematic interaction. Spherical configurations were treated within the SM-sph and the PM-sph, while deformed configurations were described using an axially deformed basis within the same QRPA framework, including both the SQP-def and the SM-def.

Table 3. Gamow–Teller (GT) transition energies (ω) and corresponding log(ft) values for the prolate-deformed ^{74}Kr nucleus, obtained within the SM-def version of the QRPA formalism, shown separately for the $K = 0$ and $K = 1$ components. $^{74}_{36}\mathrm{Kr}(0^+, \text{g.s.}) \rightarrow ^{74}_{35}\mathrm{Br}(1^+)$, $Q_{EC} = 2975$ keV.

SM-def[3]			SM-def[2]			SM-def[1]			Exp.		
ω	I	log(ft)	ω	I	log(ft)	ω	I	log(ft)	ω	I	log(ft)
	k = 0			*k = 0*			*k = 0*				
0.68	0.26	5.21	0.52	0.24	5.18	0.05	0.07	5.12	0.212	31	4.8
1.04	1.66	6.09	0.91	1.72	7.44	0.49	1.75	6.04	0.306	41	4.6
1.15	0.22	4.46	1.03	0.009	4.44	0.62	0.21	4.43	0.609	3.1	5.4
1.92	9.34	4.99	1.81	9.48	5.36	1.41	8.64	7.03	0.701	3.2	5.3
1.99	2.68	4.42	1.88	1.13	4.35	1.53	0.02	4.28	0.970	1	5.5
2.29	10.13	5.04	2.17	11.64	4.99	1.83	12.11	4.72			
2.36	2.46	5.64	2.25	2.64	5.65	1.98	4.43	8.56			
2.52	0.61	5.16	2.43	0.58	5.24	2.22	0.0006	4.66			
2.76	1.86	4.12	2.70	1.48	8.47	2.40	5.03	5.18			
			2.90	0.0008	5.21	2.66	1.52	6.81			
	k = 1			*k = 1*			*k = 1*				
0.49	20.14	5.13	0.34	1.61	5.04	0.02	0.04	4.66			
0.59	1.96	4.61	0.45	2.35	4.60	0.21	5.10	4.76			
0.78	6.52	4.72	0.63	6.51	4.70	0.60	4.02	7.48			
1.19	5.11	7.82	1.05	5.16	7.64	0.74	0.008	5.39			
1.23	0.004	5.30	1.12	0.006	6.85	0.79	0.95	4.92			
1.35	1.34	8.57	1.22	0.04	5.24	0.88	2.79	4.94			
1.38	0.0007	4.68	1.26	1.51	4.84	0.97	2.65	5.84			
1.54	5.60	5.76	1.41	3.78	5.65	0.98	0.33	6.67			
1.54	0.46	6.69	1.41	0.58	6.65	1.15	0.05	4.29			
1.69	0.05	4.68	1.56	0.06	4.49	1.29	11.75	4.62			
1.75	5.55	4.37	1.64	8.50	4.47	1.47	5.58	5.05			
1.91	11.25	4.63	1.81	8.91	4.00	1.79	2.06	5.03			
2.29	6.18	5.25	2.17	25.77	5.19	2.13	2.15	7.08			
2.48	1.50	7.45	2.38	1.67	7.80	2.21	0.02	10.77			
2.60	0.009	11.42	2.53	0.004	9.56	2.36	0.00	4.72			
2.62	0.00	8.15	2.55	0.00	8.07	2.38	4.43	7.30			
2.70	0.002	7.66	2.58	0.002	8.45	2.58	0.01	4.29			
2.85	0.006	4.72	2.78	0.0009	4.75	2.63	11.96	4.40			
2.94	5.08	4.89	2.85	4.60	4.85	2.70	9.17	4.87			
						2.82	3.15	4.09			

Note: For β^+ emission the available energy is $Q_{\beta+} = Q_{EC} - 2m_e c^2$.

Table 4. Comparison of calculated total (β^+ + EC) half-lives with the experimental value for deformed ^{74}Kr.

Models	$T_{1/2}$ (min)
Exp.	11.5
SM-def^3(p)	11.83
SM-def^2(p)	11.54
SM-def^1(p)	10.27
SM-def^3(o)	11.59
SM-def^2(o)	11.05
SM-def^1(o)	10.13

For the deformed nucleus, increasing neutron and proton pairing gaps (Δ_n, Δ_p) systematically shift the dominant GT strength to higher excitation energies and reduce the 1^+ transition strength. In spherical configurations, the effect of pairing is model dependent: within the SM-sph framework the GT strength decreases with increasing pairing gaps, whereas in the PM-sph approach the opposite trend is observed. These differences reflect the distinct treatment of residual spin–isospin correlations and symmetry restoration in the two models, and emphasize the interplay between nuclear shape and pairing correlations in governing weak-interaction observables. Microscopically, these effects arise from pairing-induced changes in quasiparticle energies and BCS occupation amplitudes, which alter both the location and collectivity of the dominant neutron–proton two–quasiparticle transitions.

The spherical calculations exhibit relatively concentrated GT strength distributions, arising from the use of spherical single–particle bases with pure *j*-shell configurations. In contrast, nuclear deformation induces strong mixing of orbitals with different *j* and *K* values, opening multiple transition channels and leading to the enhanced fragmentation observed in the SM-def results. This mechanism explains the improved agreement of the deformed calculations with the experimental GT strength distributions, particularly in terms of excitation-energy placement of the dominant peaks.

The calculated total half-lives show reasonable agreement with the experimental value. In particular, pairing gaps derived from experimental binding energies (SM-def^2) reproduce the observed half-life of ^{74}Kr with reasonable agreement. In both spherical and deformed cases, decreasing pairing gaps lead to shorter combined (β^+ + EC) half-lives, demonstrating the strong sensitivity of decay rates to pairing correlations. At the same time, the similarity of the prolate and oblate results indicates that, although deformation strongly affects the GT strength distribution and fragmentation pattern, the integrated half-life is comparatively robust against changes in nuclear shape. The best agreement with experiment is obtained for the SM-def2 prescription, for which the calculated half-life differs from the experimental value by less than 1%. In contrast, the largest deviations remain within approximately 10%, indicating an overall satisfactory description of the weak-decay properties of ^{74}Kr within the adopted QRPA framework.

An important conclusion of this study is that GT strength distributions and β-decay observables depend not only on the magnitude of the pairing gaps, but also on the experimental prescription used to constrain them. The mass-dependent prescription provides a global empirical baseline, the AME2020 five-point odd–even mass differences offer the most direct experimental constraint on ground-state pairing correlations, and the separation-energy-based prescription reflects local mass-surface effects. Even within the relatively narrow interval $\Delta \approx 1.4$–1.7 MeV relevant for ^{74}Kr, these different prescriptions lead to non-negligible variations in GT peak positions, centroids, fragmentation patterns, log(ft) values, and half-lives.

In summary, the present results demonstrate that a realistic description of GT transitions and β-decay properties in shape-coexisting nuclei such as ^{74}Kr requires nuclear deformation and pairing correlations to be treated on equal footing. The good overall agreement with experimental data, obtained without introducing an additional phenomenological quenching factor for the axial-vector coupling constant, suggests that the adopted QRPA framework provides a reasonable description of the weak-interaction observables of ^{74}Kr. However, this conclusion should be interpreted as model dependent and specific to the present nucleus and configuration space.

Acknowledgments

The author acknowledges Eskisehir Osmangazi University for providing institutional and research support.

Data availability statement

All data that support the findings of this study are included within the article (and any supplementary files).

Funding

This work was supported by Eskisehir Osmangazi University Scientific Research Projects (BAP), Project No. FBA-2025-3578.

Author contribution

Sadiye Meral Cakmak 0000-0001-9256-0571
Conceptualization (equal), Data curation (equal), Formal analysis (equal), Funding acquisition (equal), Investigation (equal), Methodology (equal), Project administration (equal), Resources (equal), Software (equal), Supervision (equal), Validation (equal), Visualization (equal), Writing – original draft (equal), Writing – review & editing (equal)

References

[1] Ericson T and Weise W 1988 *Pions and Nuclei* (Oxford Clarendon)
[2] Bertsch G F and Esbensen H 1991 Pair correlations near the neutron drip line *Ann. Phys.* **209** 327–63
[3] Bohr A and Mottelson B R 1975 *Nuclear Structure* vol 2 (W. A. Benjamin)
[4] Engel J and Vogel P 2004 Effective operators for double-β decay *Phys. Rev.* C **69** 034304
[5] Ichimura M, Sakai H and Wakasa T 2006 Spin–isospin responses via (p,n) and (n,p) reactions *Prog. Part. Nucl. Phys.* **56** 446–531
[6] Paar N, Vretenar D, Marketin T and Ring P 2003 Quasiparticle random phase approximation based on the relativistic Hartree–Bogoliubov model *Phys. Rev.* C **67** 034312
[7] Caurier E, Langanke K, Martínez-Pinedo G and Nowacki F 1999 Shell-model calculations of stellar weak interaction rates. I. Gamow–Teller distributions and spectra of nuclei in the mass range $A = 45$–65 *Nucl. Phys. A* **653** 439–52
[8] Schatz H *et al* 1998 RP-process nucleosynthesis at extreme temperature and density conditions *Phys. Rep.* **294** 167–263
[9] Marketin T, Huther L and Martínez-Pinedo G 2016 Large-scale evaluation of β-decay rates of r-process nuclei with the inclusion of first-forbidden transitions *Phys. Rev. C* **93** 025805
[10] Mustonen M T and Engel J 2016 Global calculations of β-decay rates in the QRPA framework *Phys. Rev. C* **93** 014304
[11] Langanke K and Martínez-Pinedo G 2003 Nuclear weak-interaction processes in stars *Rev. Mod. Phys.* **75** 819
[12] Caurier E, Nowacki F, Poves A and Retamosa J Poves A and Retamosa J1996 Shell model studies of the double beta decays of ^{76}Ge, ^{82}Se and ^{136}Xe *Phys. Rev. Lett.* **77** 1954–7
[13] Otsuka T, Fujimoto R, Utsuno Y, Brown B A, Honma M and Mizusaki T 2001 Magic numbers in exotic nuclei and spin–isospin properties of NN interaction *Phys. Rev. Lett.* **87** 082502
[14] Bender M, Heenen P-H and Reinhard P-G 2003 Self-consistent mean-field models for nuclear structure *Rev. Mod. Phys.* **75** 121–80
[15] Niu Z M, Niu Y F, Liang H Z, Long W H T, Vretenar D and Meng J 2013 β-decay half-lives of neutron-rich nuclei and matter flow in the R-process *Phys. Lett. B* **723** 172–6
[16] Hamamoto I 1965 Neutron–proton interaction and allowed beta-decay of G–T type *Nucl. Phys.* **62** 49–74
[17] Krumlinde J and Möller P 1984 Calculation of Gamow–Teller β-strength functions in the rubidium region in the RPA approximation with Nilsson-model wave functions *Nucl. Phys. A* **417** 419–46
[18] Möller P and Randrup J 1990 New developments in the calculation of β-strength functions *Nucl. Phys. A* **514** 1–48
[19] Frisk F, Hamamoto I and Zhang X Z 1995 Gamow–Teller β^+ decay of deformed nuclei near the proton drip line *Phys. Rev. C* **52** 2468
[20] Hamamoto I and Zhang X Z 1995 Dependence of Gamow–Teller β^+ decay of ^{80}Zr, ^{76}Sr and ^{72}Kr on nuclear shape *Z. Phys. A* **353** 145–8
[21] Borzov I N, Fayans S A and Tljykov E L 1995 Gamow–Teller strength functions of superfluid odd-A nuclei and neutrino capture reactions *Nucl. Phys. A* **584** 335–61
[22] Engel J, Bender M, Dobaczewski J, Nazarewicz W and Surman R 1999 β decay rates of r-process waiting-point nuclei in a self-consistent approach *Phys. Rev. C* **60** 014302
[23] Radha P B, Dean D J, Koonin S E, Langanke K and Vogel P 1997 Gamow–Teller strength distributions in fp-shell nuclei *Phys. Rev. C* **56** 3079
[24] Sarriguren P, Moya de Guerra E, Escuderos A and Carrizo A C 1998 β decay and shape isomerism in ^{74}Kr *Nucl. Phys. A* **635** 55–85
[25] Sarriguren P, Moya de Guerra E and Escuderos A 2001 β decay in odd-A and even-even proton-rich Kr isotopes *Phys. Rev. C* **64** 064306
[26] Poirier E 2002 *PhD Thesis* Université de Strasbourg, Internal Report No IReS-03-01
[27] Poirier E *et al* 2004 B(GT) strength from β-decay measurements and inferred shape mixing in ^{74}Kr *Phys. Rev. C* **69** 034307
[28] Petrovici A, Schmid K W and Faessler A 2000 Microscopic aspects of shape coexistence in ^{7}2Kr and ^{74}Kr *Nucl. Phys. A* **665** 333–50
[29] Petrovici A, Schmid K W and Faessler A 1996 Shape coexistence and shape transition in $N \simeq Z$ nuclei from krypton to molybdenum *Nucl. Phys. A* **605** 290–300
[30] Chandler C *et al* 1997 Evidence for a highly deformed oblate 0^+ state in $^{74}_{36}$Kr *Phys. Rev. C* **56** R2924

[31] Petrovici A, Schmid K W, Faessler A, Hamilton J H and Ramayya A V 1999 Shape coexistence phenomena in medium mass nuclei *Prog. Part. Nucl. Phys.* **43** 485–535
[32] Bender M and Heenen P H 2008 Configuration mixing of angular-momentum and particle-number projected triaxial Hartree-Fock-Bogoliubov states using the Skyrme energy density functional *Phys. Rev. C* **78** 024309
[33] Gleit C, Tang C and Coryell C 1963 Beta decay transition probabilities *Nucl. Data Sheets* **5** 5–109
[34] Raman S and Gove N 1973 Rules for spin and parity assignments based on log(*ft*) values *Phys. Rev. C* **7** 1995–2009
[35] Singh B, Rodriguez J L, Wong S S M and Tuli J K 1993 Review of log(*ft*) values in β decay *Nucl. Data Sheets* **84** 487–556
[36] Petrovici A, Schmid K W, Radu O and Faessler A 2008 Gamow–Teller β decay of ^{74}Kr in a self-consistent approach *Nucl. Phys. A* **799** 94–104
[37] Ullah A, Nabi J-U and Tahir M 2023 Investigation of effects of pairing correlations on calculated β-decay half-lives of FP-shell nuclei *Braz. J. Phys.* **53** 39
[38] Pyatov N I and Salamov D 1977 Conservation laws and collective excitations in nuclei *Nucleonica* **22** 127–41
[39] Salamov D, Kucukbursa A, Maraş I, Aygör H, Babacan T and Bircan H 2003 Calculation of the log(*ft*) values for the allowed Gamow–Teller transitions in deformed nuclei using the basis of Woods–Saxon wave functions *Acta Phys. Slov.* **53** 307–19
[40] Cakmak S, Nabi J-U, Babacan T and Selam C 2014 Study of Gamow–Teller transitions in isotopes of titanium within the quasiparticle random phase approximation *Astrophys. Space Sci.* **352** 645–63
[41] Salamov D I *et al* 2006 *Proc. 5th Conf. Nucl. Part. Phys.* vol **361** (*Cairo*: NUPPAC)
[42] Ikeda K I 1964 Collective excitation of unlike pair states in heavier nuclei *Prog. Theor. Phys.* **31** 434–51
[43] Babacan T, Salamov D I and Kucukbursa A 2005 Gamow–Teller 1^+ states in ^{208}Bi *Phys. Rev.* C **71** 037303
[44] Babacan T, Salamov D I and Kucukbursa A 2005 The investigation of the log(*ft*) values for the allowed Gamow–Teller transitions of some deformed nuclei *Math. Comput. Appl.* **10** 359–68
[45] Cakmak N, Unlu S and Selam C 2010 Gamow–Teller 1^+ states in 112 Sb–^{124} Sb isotopes *Pramana J. Phys.* **75** 649–63
[46] Selam C, Babacan T, Aygör H A, Bircan H, Kuçukbursa A and Maraş I 2004 Investigation of the log(*ft*) values for allowed Gamow–Teller transitions of some deformed nuclei *Math. Comput. Appl.* **9** 79–90
[47] Wang M, Huang W J, Kondev F G, Audi G and Naimi S 2021 The AME 2020 atomic mass evaluation (II) *Chin. Phys. C* **45** 030003
[48] NNDC NuDat 2.8 database
[49] Homma H, Bender E, Hirsch M, Muto K, Klapdor-Kleingrothaus H V and Oda T 1996 Systematic study of nuclear β decay *Phys. Rev. C* **54** 2972
[50] Cakmak S M 2026 Gamow–Teller transitions and β-decay properties of ^{74}Kr: effects of deformation and residual interactions *Acta Phys. Pol. B* **57** 3–A2
[51] Möller P and Nix J R 1981 Atomic masses and nuclear ground-state deformations calculated with a new macroscopic-microscopic model *At. Data Nucl. Data tables* **26** 165–96
[52] Möller P, Nix J R, Myers W D and Swiatecki W J 1995 Nuclear ground-state masses and deformations *At. Data Nucl. Data tables* **59** 185–381
[53] Warburton E K, Towner I S and Brown B A 1994 First-forbidden β decay: meson-exchange enhancement of the axial charge at *A* 16 *Phys. Rev. C* **49** 824–39
[54] Suhonen J 2007 *From Nucleons to Nucleus: Concepts of Microscopic Nuclear Theory* (Springer)
[55] Surender K V and Srivastava P C 2024 Study of β^+/EC-decay properties of shell nuclei using nuclear shell model *Ann. Phys.* **470** 169772
[56] Kondev F G, Wang M, Huang W J, Naimi S and Audi G 2021 The NUBASE2020 evaluation of nuclear physics properties *Chin. Phys. C* **45** 030001
[57] Audi G and Wapstra A H 1995 The 1995 update to the atomic mass evaluation *Nucl. Phys. A* **595** 409–80
[58] Audi G, Bersillon O, Blachot J and Wapstra A H 1997 The NUBASE evaluation of nuclear and decay properties *Nucl. Phys. A* **624** 1–124